



Turbulence Effects on Precipitation and Cloud Radiative Properties in Shallow Cumulus: an Investigation Using the WRF-LES Model Coupled with Bin Microphysics

Hyunho Lee^{1,2,3} · Jong-Jin Baik¹ · Alexander P. Khain⁴

Received: 18 August 2017 / Revised: 8 January 2018 / Accepted: 17 January 2018 / Published online: 30 August 2018
© Korean Meteorological Society and Springer Nature B.V. 2018

Abstract

Using the large-eddy simulation version of the Weather Research and Forecasting (WRF) model coupled with a detailed bin microphysics scheme, the effects of turbulence-induced collision enhancement (TICE) on precipitation and cloud radiative properties in shallow cumulus are investigated. Similar to previous studies, the enhanced droplet collision results in an increase in rainwater content and surface precipitation amount. However, under low aerosol number concentration, the relative frequency of large surface precipitation amount is decreased mainly due to the decreased condensation amount. Due to TICE, the mean drop size increases and the drop number concentration decreases, which results in a decrease in evaporation and hence increasing cloud fraction. However, these changes induce a decrease in cloud optical thickness which largely offsets the increased cloud fraction when the domain-averaged albedo is calculated. Similarly, a decrease in cloud top height caused by the decreased in-cloud vertical velocity largely offsets the increased cloud fraction when the domain-averaged outgoing longwave radiation is calculated. Therefore, the effects of TICE on cloud radiative properties in shallow cumulus do not appear prominently. In addition, TICE results in a decrease in the shear production of turbulent kinetic energy, which indicates that TICE acts to produce a negative feedback.

Keywords Turbulence-induced collision enhancement (TICE) · Bin microphysics · Shallow cumulus · Precipitation · Cloud radiative properties

1 Introduction

Warm clouds, which consist of liquid drops, cover a large portion of the atmosphere and greatly influence the Earth's weather and climate. Despite their seeming simpleness, however, uncertainties in treating warm clouds in weather and

climate models are large because complex and various physical processes occur inside and around the clouds and many environmental conditions affect the development of the clouds. There are many factors that make accurate simulations of warm clouds difficult. Turbulence is regarded as one of the factors because a few millimeter of grid size is required to fully resolve turbulence.

Turbulence can enhance the collision rate of drops mainly by 1) introducing a difference in velocity of drops which have a similar or the same size and hardly collide with each other, 2) causing a change in airflow around drops and aerodynamic interaction between drops, and 3) generating a preferential drop concentration. A more detailed discussion can be found in Grabowski and Wang (2013). Turbulence is known to enhance the collision rate between drops up to several times depending on turbulence intensity and drop size (Franklin et al. 2005; Pinsky et al. 2008; Ayala et al. 2008; Wang and Grabowski 2009; Kunnen et al. 2013), hence affecting precipitation in warm clouds (Franklin 2008, 2014; Seifert et al. 2010; Riechelmann et al. 2012; Wyszogrodzki et al. 2013; Lee et al. 2015).

Responsible editor: Ben Jong-Dao Jou, PhD

✉ Hyunho Lee
hyunho.lee@nasa.gov

¹ School of Earth and Environmental Sciences, Seoul National University, Seoul 08826, South Korea

² Center for Climate Systems Research, Columbia University, New York, NY 10025, USA

³ NASA Goddard Institute for Space Studies, New York, NY 10025, USA

⁴ Department of Atmospheric Sciences, The Hebrew University of Jerusalem, 91904 Jerusalem, Israel

Using a large-eddy simulation (LES) model with bulk microphysics, Seifert et al. (2010) demonstrated that this turbulence effect in shallow cumulus is evident on rain measures but other cloud-related properties (e.g., cloud cover, cloud water path, cloud top height) are less affected by the turbulence effect. Using an LES model with bin microphysics, Wyszogrodzki et al. (2013) also showed that the surface precipitation in shallow cumulus increases up to several times by the turbulence effect but the cloud water path exhibits similar levels regardless of whether the turbulence effect is considered. Using a two-dimensional cloud model with bin microphysics, Lee et al. (2015) demonstrated that the impacts of turbulence effect on surface precipitation in shallow cumulus depend on aerosol number concentration and low-level humidity. According to Lee et al. (2015), the surface precipitation can be reduced by the turbulence effect under the conditions of low aerosol number concentration and high humidity. Wyszogrodzki et al. (2013) and Grabowski et al. (2015) argued that the turbulence effect produces a positive feedback, i.e., the turbulent kinetic energy increases due to the turbulence effect by increased buoyancy and raised cloud top height in maritime shallow cumulus. Franklin (2014) noted that whether the turbulence effect produces a positive or negative feedback depends on cloud type (stratocumulus or shallow cumulus) and the vertical location in the clouds.

Many previous studies have focused on the impacts of the turbulence effect on surface precipitation (e.g., Seifert et al. 2010; Wyszogrodzki et al. 2013; Franklin 2014), but there have been relatively few studies that investigate the impacts of the turbulence effect on cloud radiative properties. This study aims to examine how the turbulence effect affects not only surface precipitation but also cloud radiative properties, such as cloud fraction, albedo, and outgoing longwave radiation of shallow cumulus. This study also aims to examine the impacts of the turbulence effect on the feedback between cloud and precipitation (e.g., Xue et al. 2008; Feingold et al. 2010; Koren and Feingold 2011) and on the feedback between cloud and turbulence (Wyszogrodzki et al. 2013; Franklin 2014). For these purposes, using an LES model coupled with a detailed bin microphysics scheme, shallow cumulus under idealized atmospheric conditions and in the presence of a temperature inversion layer is simulated and analyzed in detail.

The numerical model used in this study and the experimental setup are described in Section 2. The simulation results are presented and discussed in Section 3. A summary and conclusions are provided in Section 4.

2 Model Description and Experimental Setup

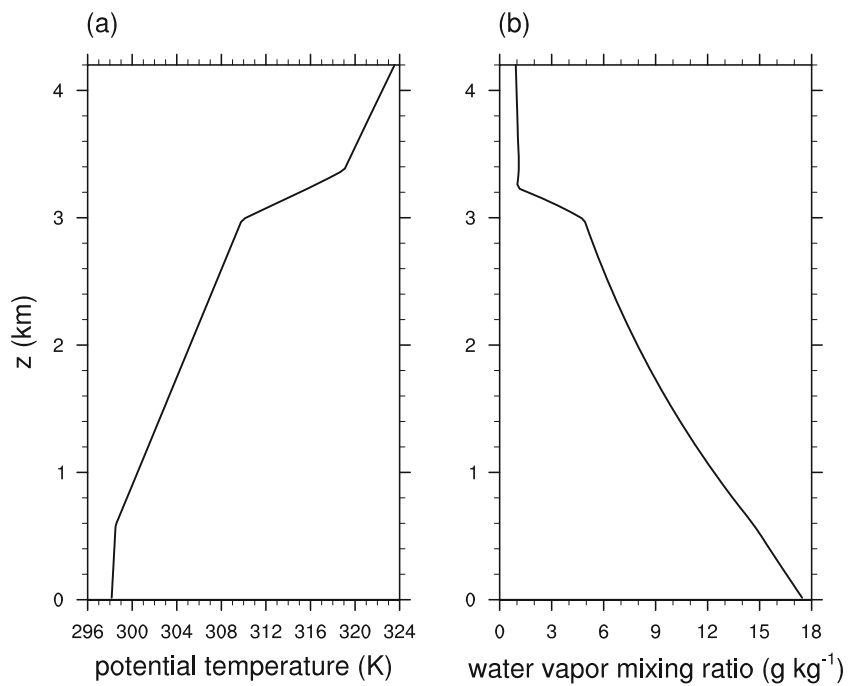
The LES version of the Weather Research and Forecasting (WRF) model version 3.7.1 (Skamarock et al. 2008) is used in this study. The bin microphysics scheme of the Hebrew

University Cloud Model (HUCM, Khain et al. 2011) is incorporated into the WRF model (Lee and Baik 2016, 2017). This microphysics scheme uses 43 mass-doubling bins to represent the size distribution of each hydrometeor type and aerosol. Although the original version of this microphysics scheme includes many ice microphysical processes, the modified version used in this study considers only warm cloud microphysical processes, that is, nucleation, vapor diffusion (condensation and evaporation), collision, breakup, and sedimentation processes.

All aerosol particles are assumed to serve as cloud condensation nuclei (CCN). Aerosol particles whose radii are larger than a critical radius are activated into droplets, and the radius of the activated droplet is determined by the radius of aerosol particle (Khain et al. 2000). The Köhler equation (Köhler 1936) is used to calculate the critical aerosol radius for a given grid-scale supersaturation. The typical equation of vapor diffusion process (Pruppacher and Klett 1997; Houze Jr. 2014) with the curvature and solution effects neglected is used. An analytic approach to consider a change in relative humidity within a time step is utilized (Khain et al. 2008). A redistribution method that conserves both the number and mass of drops is applied to treat the drops that have arbitrary mass due to the vapor diffusion process in the regular mass bin grid. The exponential flux method developed by Bott (2000) which is numerically efficient, conserves mass exactly, and reduces numerical diffusion is applied to solve the stochastic collection equation with the pressure-dependent collision efficiencies obtained by Pinsky et al. (2001). The coalescence efficiencies provided by Low and List (1982) and Beard and Ochs (1995) are used. The parameterization of breakup process is realized using the method proposed by Bleck (1970). An implicit time integration method and sub-time steps are considered in the breakup process to ensure that the drop concentration remains positive and to conserve the total water mass, respectively. The breakup process in the HUCM microphysics scheme is described in detail by Seifert et al. (2005). Drop sedimentation is evaluated using a forward explicit upwind scheme with the drop terminal velocity parameterized as a function of drop radius following Beard (1976).

To consider the turbulence-induced collision enhancement (TICE) between drops, the result of Pinsky et al. (2008), which is obtained using a turbulence statistical model, is adopted by the microphysics scheme. The result of Pinsky et al. (2008) is similar to that obtained using direct numerical simulation models (Grabowski and Wang 2013). TICE is tabulated in 11 tables according to the combinations of the turbulence dissipation rate and the Taylor microscale Reynolds number. The turbulence parameters (turbulent dissipation rate and Taylor microscale Reynolds number) are diagnosed using the turbulent kinetic energy (TKE). The 1.5th order turbulent closure scheme is used to predict TKE in the WRF model (Skamarock et al. 2008). A detailed procedure to calculate

Fig. 1 Vertical profiles of the initial (a) potential temperature and (b) water vapor mixing ratio used in this study, which are slightly modified from those of Ogura and Takahashi (1973)

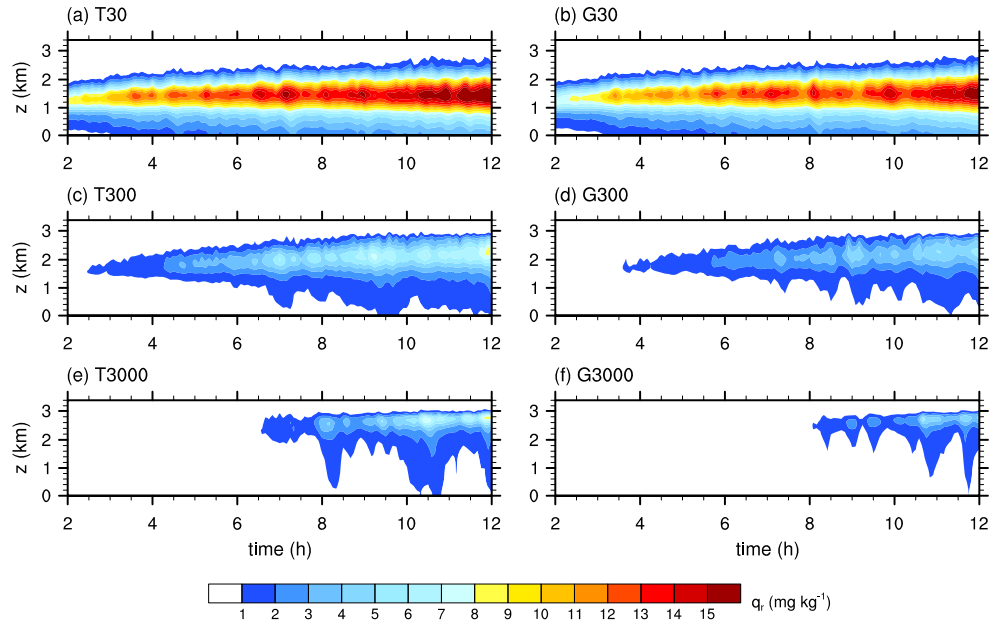


the turbulence parameters from TKE is described by Benmoshe et al. (2012), except that in this study the external cloud length scale and the total (cloud scale) TKE are replaced by the turbulent mixing length and TKE at each grid point, respectively (Lee and Baik 2016).

In this study, the thermodynamic sounding over the tropical ocean for typical maritime shallow cumulus in Ogura and Takahashi (1973) is adopted. The original sounding is slightly modified so that water vapor mixing ratio is nearly constant with height above the inversion layer (Fig. 1). A strong

temperature inversion layer is lain on $z = 3\text{--}3.4$ km, where the temperature is $\sim 6^\circ\text{C}$. The basic-state wind is set to be calm in the entire model domain (Wang and Feingold 2009). A constant surface heat flux of $1.2 \times 10^{-2} \text{ K m s}^{-1}$ and a constant surface water vapor flux of $3.4 \times 10^{-5} \text{ m s}^{-1}$ (approximately 15 and 100 W m^{-2} , respectively) are applied for bottom boundary conditions. Large-scale subsidence is provided using a uniform horizontal divergence of $3.75 \times 10^{-6} \text{ s}^{-1}$ multiplied by the altitude (Wang and Feingold 2009). The subsidence velocity at higher altitudes is limited to 0.5 cm s^{-1}

Fig. 2 Time evolution of horizontally averaged rainwater content in (a) T30, (b) G30, (c) T300, (d) G300, (e) T3000, and (f) G3000



(vanZanten et al. 2011). Random perturbations of $[-0.3 \text{ K}, 0.3 \text{ K}]$ are added to the initial potential temperature field at the lowest 4 model levels. The Coriolis force is neglected.

The initial aerosol size distribution follows the Twomey equation (Twomey 1959), as in Khain et al. (2000) and Lee et al. (2015). The aerosol number concentration is set for the CCN number concentration at 1% supersaturation (N_0) to be 30, 300, and 3000 cm^{-3} . Six numerical experiments (T30, G30, T300, G300, T3000, and G3000) are conducted according to the collision kernel type ('T' and 'G' denote the turbulent and gravitational collision kernel, respectively) and the aerosol number concentration (N_0 of 30, 300, and 3000 cm^{-3}). The aerosol number concentration is constant below $z = 2 \text{ km}$ and decreases exponentially with height above $z = 2 \text{ km}$ with an e -folding depth of 2 km. The aerosol replenishment scheme proposed by Jiang and Wang (2014) is adopted with a time scale of 1 h.

To examine the effects of TICE reliably, it would be better to perform many numerical simulations and make an ensemble averaging. In this study, each of the six experiments is performed three times by changing only the initial random perturbations to the potential temperature field. Although the number of ensemble members is somewhat limited, the trend of the effects of TICE is found to be the same across all the ensemble members. All quantities are analyzed with the ensemble averaging.

The domain size is $20 \text{ km} \times 20 \text{ km} \times 4.2 \text{ km}$. Periodic boundary conditions are applied in both the x and y directions. A sponge layer is put from $z = 3.4$ to 4.2 km . The grid size is 100 m in the horizontal and 30 m in the vertical, similar to that used in previous studies (e.g., Seifert et al. 2010; Wyszogrodzki et al. 2013; Franklin 2014). The integration period is 12 h from 18:00 LT (local time). The time step is 1 s except for the vapor diffusion process (0.5 s) and the breakup process (variable). Except the microphysics scheme, only the RRTM longwave radiation scheme (Mlawer et al.

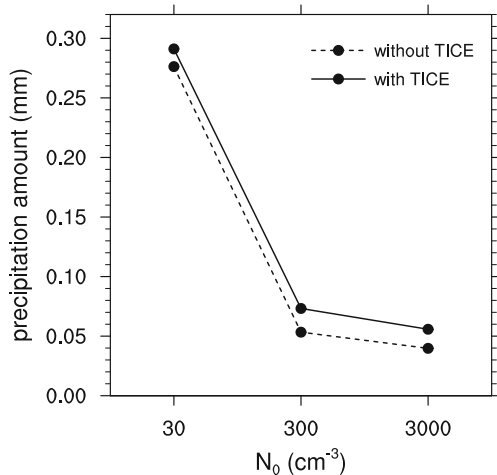


Fig. 3 Amount of accumulated surface precipitation averaged over the domain for $t = 2\text{--}12 \text{ h}$

1997) is employed for physics parameterization. Note that a simple discussion on the effects of shortwave radiation on shallow convection is found in Feingold et al. (2015).

3 Results and Discussion

3.1 Effects of TICE on Precipitation

Figure 2 shows the time evolution of horizontally averaged rainwater content. In T30 and G30, the rainwater content is generally large compared to the other cases and the vertical

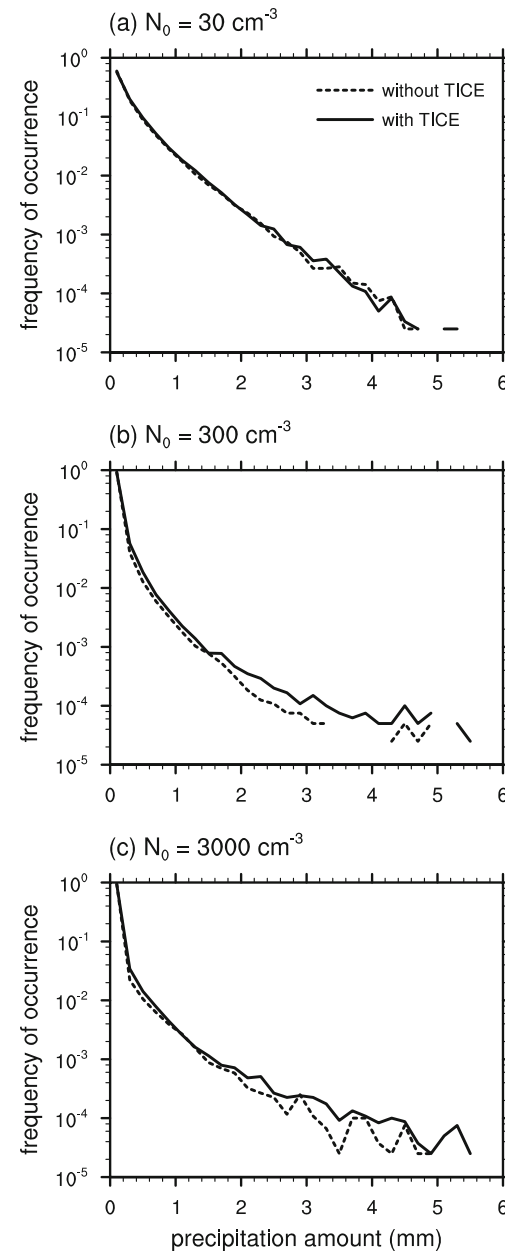


Fig. 4 Probability density function of accumulated surface precipitation amount for $t = 2\text{--}12 \text{ h}$. $N_0 =$ (a) 30 cm^{-3} , (b) 300 cm^{-3} , and (c) 3000 cm^{-3}

extent of raindrop distribution does not reach 3 km that is the base height of the inversion layer. The amount of rainwater content is larger in T30 than in G30, but the difference is small. On the other hand, when $N_0 = 300$ and 3000 cm^{-3} , the vertical extent of raindrop distribution is relatively high and the rainwater content is relatively small compared to the cases with $N_0 = 30 \text{ cm}^{-3}$. It is clearly observed that TICE increases rainwater content under these relatively high aerosol number concentrations.

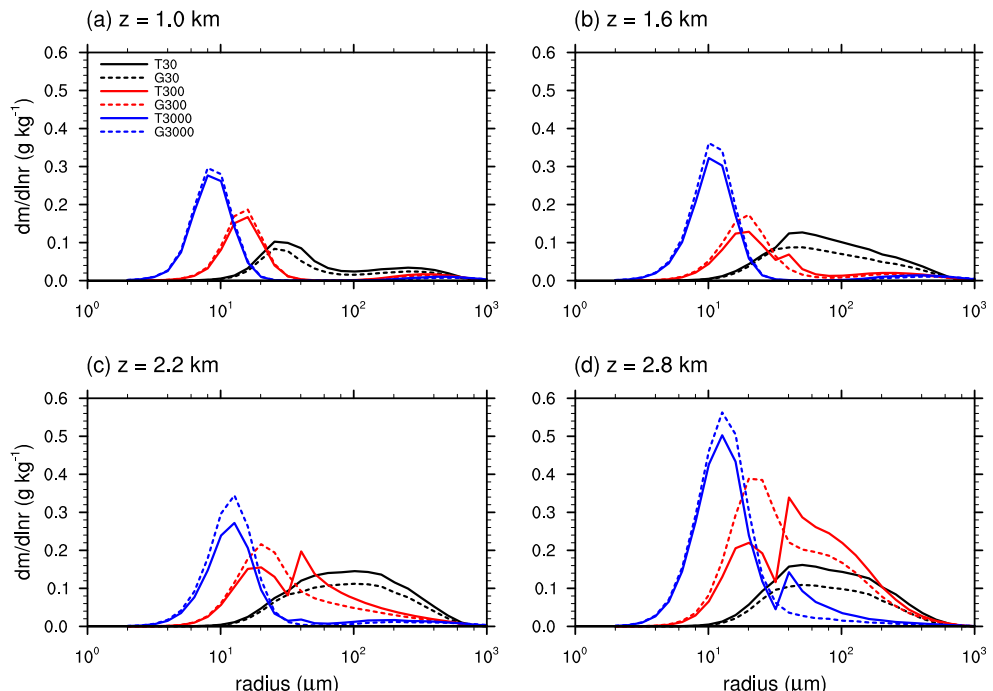
The increase in rainwater content can be explained by the enhanced drop growth, which agrees with the results of previous studies (e.g., Seifert et al. 2010; Wyszogrodzki et al. 2013; Franklin 2014; Lee et al. 2015). The TICE-induced increase in rainwater content is more distinct as the aerosol number concentration is higher, which agrees with the result of Lee et al. (2015). According to Lee et al. (2015), in the highly humid environmental conditions, the effects of TICE on the rainwater content are less pronounced under lower aerosol number concentration because raindrops can be formed more easily even without the consideration of TICE. It is shown in Fig. 2 that the effects of TICE on the rainwater content tend to be opposite to the effects of increase in aerosol number concentration on the rainwater content, which agrees with the results of Benmoshe et al. (2012) and Lee et al. (2015).

Figure 3 shows the surface precipitation amount accumulated over almost the entire integration period, $t = 2\text{--}12 \text{ h}$. First an increase in aerosol number concentration substantially decreases surface precipitation amount. It is also clearly seen that the surface precipitation amount increases due to TICE under

all aerosol number concentrations considered in this study, which agrees with the results of some previous studies (Seifert et al. 2010; Wyszogrodzki et al. 2013). The relative increase in surface precipitation amount due to TICE is larger as the aerosol number concentration is higher; it is approximately 5% when $N_0 = 30 \text{ cm}^{-3}$, whereas it is approximately 40% when $N_0 = 3000 \text{ cm}^{-3}$.

The relative frequency distribution of accumulated surface precipitation amount is shown in Fig. 4. When $N_0 = 300$ and 3000 cm^{-3} , the relative frequency of accumulated surface precipitation amount is higher in the case with TICE than in the case without TICE across almost the whole range of surface precipitation amount. This is reflected in the TICE-induced increased surface precipitation amount (Fig. 3). However, when $N_0 = 30 \text{ cm}^{-3}$, in the range where the accumulated surface precipitation amount is relatively large (between 3.4 mm and 4.4 mm), the relative frequency of accumulated surface precipitation amount is lower in T30 than in G30, although the averaged surface precipitation amount is larger in T30 than in G30. Lee et al. (2015) suggested that the surface precipitation amount can be decreased due to TICE in a humid and clean environmental condition, mainly because TICE induces more rapid drop growth but it causes a decrease in condensational growth that is proportional to the first moment of drop size distribution (see Appendix). In this study, the condensation amount in the strong updraft core areas (vertical velocity exceeding 2 m s^{-1}) decreases due to TICE by approximately 4.5% when $N_0 = 30 \text{ cm}^{-3}$, which is similar to the result in Lee et al. (2015). Because strong surface precipitation is affected by not only collision but also condensation, the

Fig. 5 Drop size distributions at $z =$ (a) 1.0, (b) 1.6, (c) 2.2, and (d) 2.8 km averaged over the cloudy grids and the last 3 h



decreased condensation due to TICE in the strong updraft core areas plays a role in decreasing the relative frequency of large surface precipitation amount.

Drop size distributions at certain selected altitudes are shown in Fig. 5. The effects of TICE on the drop size distribution are easily observed at all the selected altitudes. The differences due to TICE become smaller as the altitude is closer to the cloud base (Fig. 5a) because the clouds consist mainly of nucleated small droplets and the turbulence intensity is relatively weak near the cloud base (Seifert et al. 2010; Lee et al. 2015). When $N_0 = 30 \text{ cm}^{-3}$, the effects of TICE on the drop size distribution is relatively small (Fig. 5b-d). When $N_0 = 300$ and 3000 cm^{-3} , in the radius range of relatively small

droplets, the critical point at which the local maximum of drop number concentration appears is almost unchanged although TICE is considered. Instead, TICE makes another critical point in the radius range of relatively large drops so the drop size distribution has a bimodal form due to TICE. Note that Berry and Reinhardt (1974) have shown that a bimodal form of drop size distribution can be seen in a condition favorable for drop collision. On the other hand, when TICE is not considered, the effects of aerosol number concentration on the drop size distribution appear to shift the critical point so the form of the drop size distribution remains unimodal. Therefore, the effects of TICE on the drop size distribution are different from the effects of decrease in aerosol number

Fig. 6 (a) Cloud optical thickness, (b) albedo, (c) cloud top height, (d) outgoing longwave radiation (OLR), and (e) cloud fraction averaged over the last 3 h. Cloud optical thickness and cloud fraction are averaged over the cloudy columns in which the liquid water path is larger than 10 g m^{-2} . Albedo and OLR are averaged over the domain assuming that the albedo of cloud-free surface is 0.08

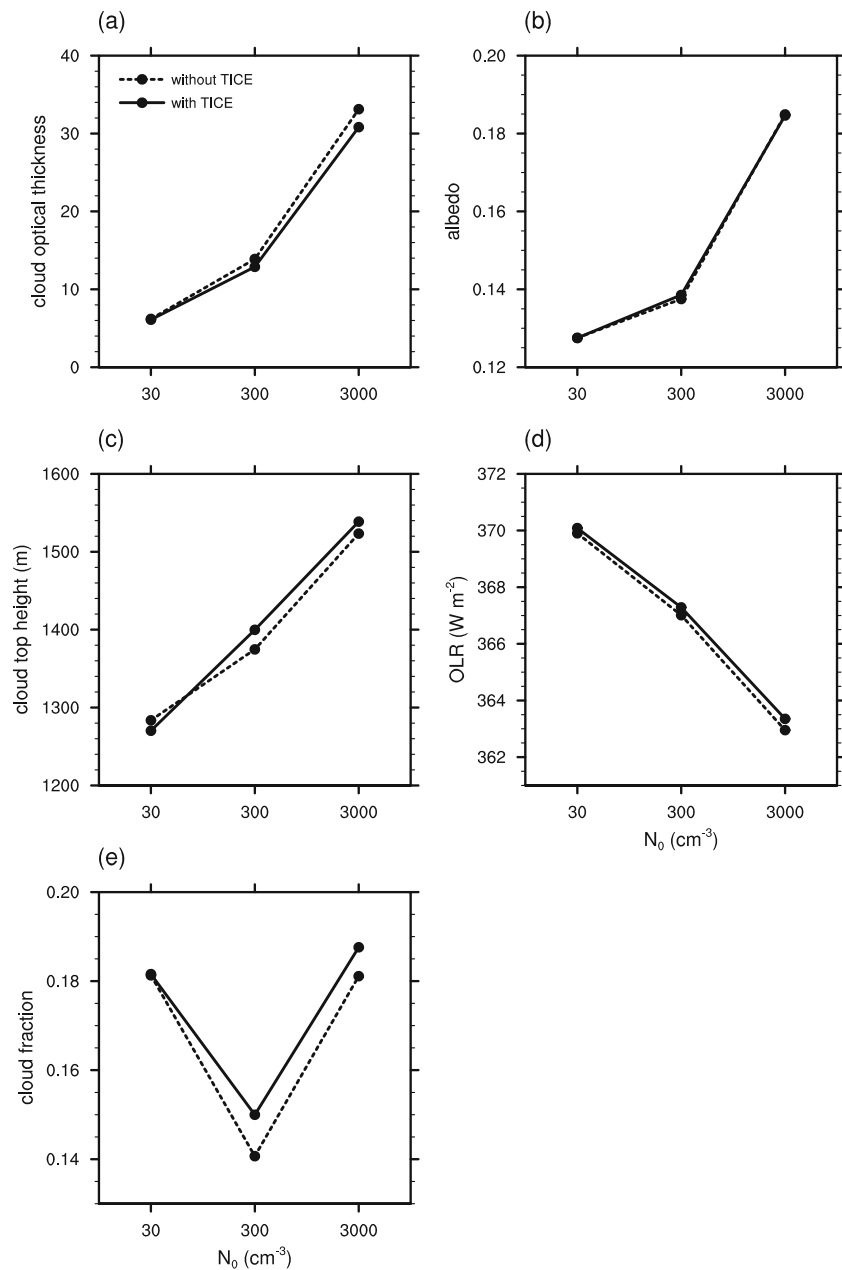
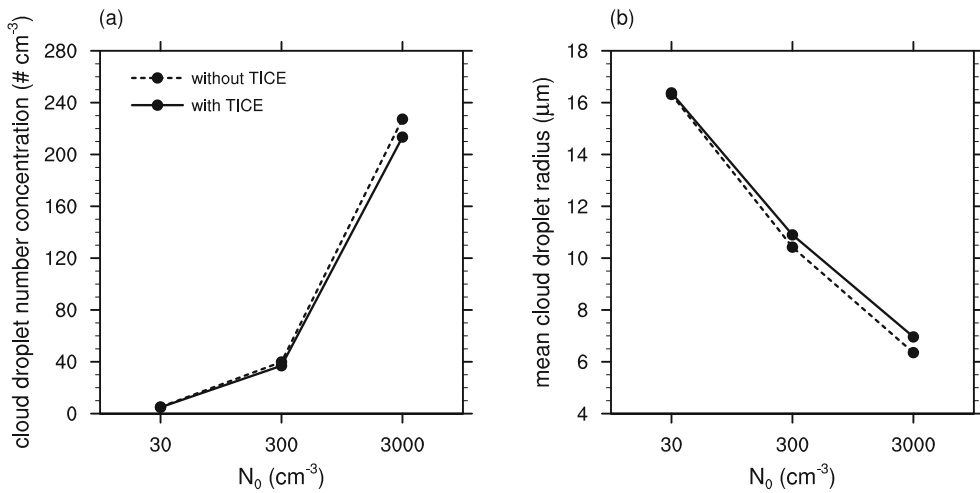


Fig. 7 (a) Cloud droplet number concentration and (b) mean cloud droplet radius averaged over the cloudy grids and the last 3 h



concentration on the drop size distribution, although both effects on the rainwater content and on the surface precipitation appear similarly (Figs. 2 and 3; Benmoshe et al. 2012; Lee et al. 2015).

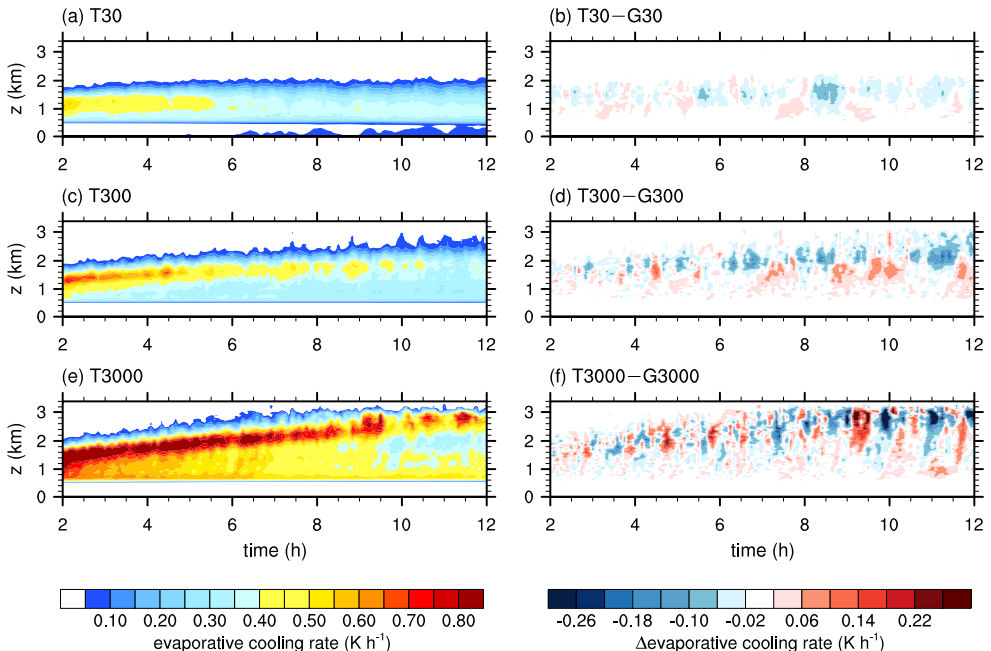
3.2 Effects of TICE on Cloud Radiative Properties

To examine the effects of TICE on cloud radiative properties, the domain-averaged albedo and outgoing longwave radiation (OLR) and the properties related to them are analyzed. Although it is thought that high clouds are more important for OLR than low and middle clouds due to their high cloud top height and that low and middle clouds play a role in scattering shortwave radiation, some studies have pointed out that low and middle clouds also contribute to the Earth's OLR budget (e.g., Costa and Shine 2006). Figure 6 shows the cloud

optical thickness, albedo, cloud top height, OLR, and cloud fraction averaged over the last 3 h. Cloud optical thickness and cloud fraction are averaged over the cloudy columns in which the liquid water path is larger than 10 g m^{-2} . Albedo and OLR are averaged over the domain with assuming that the surface albedo is 0.08 (Feingold et al. 2016). The cloud albedo is diagnosed using the cloud optical thickness proposed in Zhang et al. (2005). The cloud top height is determined as the height of the top of cloudy grids in which the cloud water content is larger than 0.01 g kg^{-1} .

Due to TICE, the cloud optical thickness is slightly decreased (Fig. 6a). First this is because of the more rapid growth of small droplets to large drops and consequent increased sedimentation. Moreover, the decrease in cloud optical thickness due to TICE is also caused by a decrease in the second moment of drop size distribution because in the cases with TICE

Fig. 8 Time evolution of horizontally averaged evaporative cooling rate in (a) T30, (c) T300, and (e) T3000. (b), (d), and (f) show the differences between T30 and G30, T300 and G300, and T3000 and G3000, respectively



the mean drop radius increases but the drop number concentration decreases (Fig. 7, also see Appendix). Combining these two factors, the cloud optical thickness decreases due to TICE, and the decrease is more pronounced under higher aerosol number concentration.

In spite of the decrease in cloud optical thickness, however, the domain-averaged albedo increases due to TICE, but the increase is very small (Fig. 6b). This increase in the domain-averaged albedo is largely due to the increase in cloud fraction (Fig. 6e). Note that cloud fraction shows a local minimum when $N_0 = 300 \text{ cm}^{-3}$ mainly due to competing of sedimentation and evaporation. Under higher aerosol number concentration, cloud fraction can be either larger due to decreased sedimentation or smaller due to increased evaporation.

To investigate possible reasons for the increase in cloud fraction, evaporation is examined. Figure 8 shows the time evolution of horizontally averaged evaporation in the cases with TICE and differences in evaporation between the cases with and without TICE. It is seen that the evaporation is generally concentrated near the cloud top and is larger for higher aerosol number concentration. Although an alternating structure is seen, evaporation generally decreases due to TICE. The decrease in cloud water content and the decrease in the first moment of drop size distribution to which evaporation is proportional are largely responsible for the decrease in evaporation. Because evaporation mainly occurs in the peripheral of clouds, the decrease in evaporation contributes to the increase in cloud fraction.

The increase in cloud fraction offsets the decrease in cloud optical thickness for diagnosing the domain-averaged albedo. In other words, the cloud optical thickness of individual clouds tends to decrease but the area occupied by clouds increases due to TICE. Thus, the domain-averaged albedo is hardly affected by TICE. The relative frequency distribution of cloud albedo shows that although the overall difference is very small, the relative frequency of large cloud albedo (larger than ~ 0.85) decreases but that of small to moderate cloud albedo (smaller than ~ 0.85) increases due to TICE (Fig. 9).

Due to TICE, the cloud top height is slightly decreased (Fig. 6c). The decrease in cloud top height due to TICE can be caused by the increased drop size and the subsequent increased sedimentation. To investigate possible dynamic causes for the decrease in cloud top height in addition to the increased sedimentation, vertical velocity is examined. Figure 10a shows the in-cloud vertical velocity averaged over the last 3 h. While the vertical velocity averaged over the clouds are positive except near the cloud top under relatively high aerosol number concentrations, TICE decreases the vertical velocity, hence contributing to the decrease in cloud top height. It is also shown that the vertical velocity variance is also slightly decreased due to TICE (Fig. 10b). This causes a decrease in in-cloud turbulence motion, which will be discussed in section 3.3.

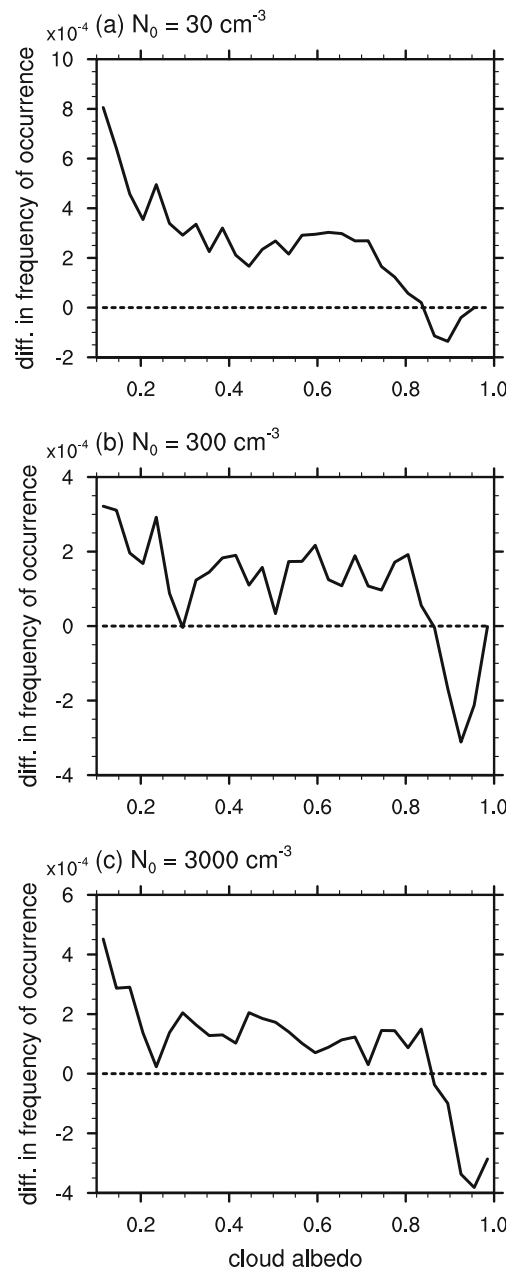
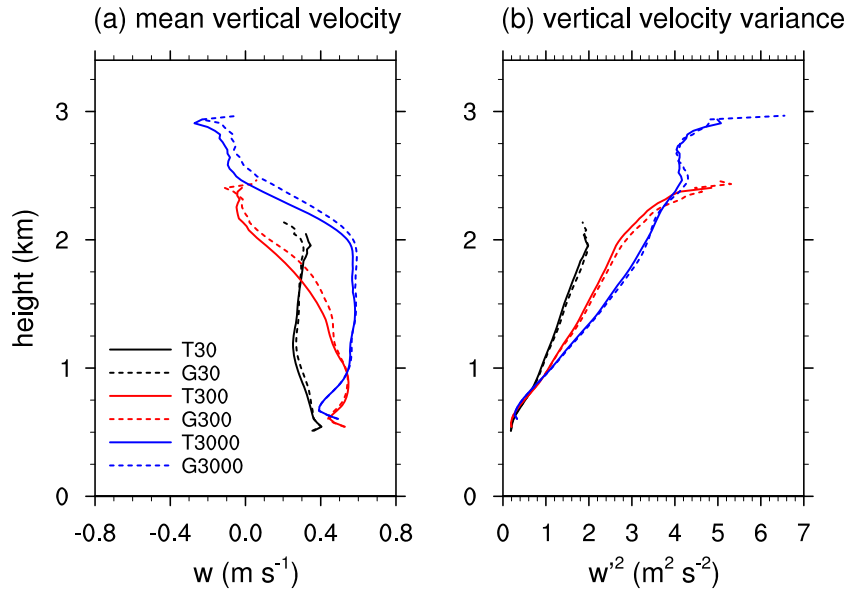


Fig. 9 Probability density function of cloud albedo calculated for the last 3 h. $N_0 =$ (a) 30 cm^{-3} , (b) 300 cm^{-3} , and (c) 3000 cm^{-3}

Figure 11 shows the vertical profiles of temperature difference between the cloudy grids and cloud-free grids and in-cloud temperature difference induced by TICE. The evaporative cooling near the cloud top is remarkable (Figs. 11a–c), and TICE reduces the evaporative cooling (Figs. 11d–f, also see Fig. 8). Therefore, the in-cloud atmosphere is less destabilized in the cases with TICE than in the cases without TICE, hence decreasing the in-cloud vertical velocity and cloud top height. Wyszogrodzki et al. (2013) and Grabowski et al. (2015) noted that the cloud top height is raised by TICE due to the decreased hydrometeor drag in shallow cumulus whose depth is $\sim 1 \text{ km}$ developing in the inversion-free

Fig. 10 Vertical profiles of (a) mean vertical velocity and (b) vertical velocity variance averaged over the cloudy grids and for the last 3 h



atmosphere. On the other hand, Franklin (2014) showed that a decrease in cloud top height is seen in shallow cumulus whose depth is ~ 2 km. In this study, the cloud depth is approximately 2–3 km, which is similar to that in Franklin (2014).

The decrease in cloud top height due to TICE can induce an increase in OLR. However, it is shown that the change in OLR is not large (Fig. 6d). Although the cloud top height decreases, the cloud fraction increases (Fig. 6e). This increase in cloud fraction offsets the decrease in cloud top height so the OLR averaged over the domain is almost unchanged by TICE.

In summary, due to TICE, the cloud optical thickness and the cloud top height decrease, but the cloud fraction increases. Because of the offsets, the effects of TICE on the domain-averaged albedo and OLR are revealed to be small under the environmental conditions considered in this study.

3.3 Effects of TICE on Feedback

Recently, there have been a few studies that reports whether turbulence intensity increases or decreases due to TICE. Wyszogrodzki et al. (2013) and Grabowski et al. (2015) reported a positive feedback, that is, turbulence intensity increases by considering TICE. On the other hand, Franklin (2014) reported that the feedback depends on the cloud thickness; it is positive in relatively shallow warm clouds but negative in relatively deep warm clouds.

The feedback of TICE is examined in this study. Figure 12 shows the turbulent kinetic energy (TKE) averaged in the clouds and the terms that contribute to the tendency of in-cloud TKE. The governing equation for TKE is expressed as (Skamarock et al. 2008)

$$\frac{\partial k}{\partial t} + \mathbf{u} \cdot \nabla k = P_s + P_b - \varepsilon, \quad (1)$$

$$P_s = K \left[\left(2 \frac{\partial u}{\partial x} \right)^2 + \left(2 \frac{\partial v}{\partial y} \right)^2 + \left(2 \frac{\partial w}{\partial z} \right)^2 + \left(\frac{\partial u}{\partial y} + \frac{\partial v}{\partial x} \right)^2 + \left(\frac{\partial v}{\partial z} + \frac{\partial w}{\partial y} \right)^2 + \left(\frac{\partial w}{\partial x} + \frac{\partial u}{\partial z} \right)^2 \right], \quad (2)$$

$$P_b = -KN^2, \quad (3)$$

$$\varepsilon = \frac{Ck^{3/2}}{l}, \quad (4)$$

Here, k is TKE, \mathbf{u} is the velocity vector, P_s , P_b , and ε represent the shear production, buoyancy production (or loss), and turbulence dissipation rate, respectively, u , v , and w are the velocities in the x , y , and z directions, respectively, and N is the buoyancy frequency. Following Skamarock et al. (2008), K , C , and l are determined using

$$K = C_k l k^{1/2}, \quad (5)$$

$$C = 1.9C_k + (0.93 - 1.9C_k) \frac{l}{\Delta s}, \quad (6)$$

$$l = \begin{cases} \min(\Delta s, 0.76k^{1/2}/N), & \text{for } N^2 > 0 \\ \Delta s, & \text{for } N^2 \leq 0 \end{cases} \quad (7)$$

where $C_k = 0.2$ and $\Delta s = (\Delta x \Delta y \Delta z)^{1/3}$ in which Δx , Δy , and Δz are the grid sizes in the x , y , and z directions, respectively.

Figure 12 shows that TKE is smaller in the cases with TICE than in the cases without TICE. This means that TICE acts as a negative feedback, which agrees with the result in Franklin (2014). The contribution of each term to TKE exhibits that the shear production is predominant over the advection and the

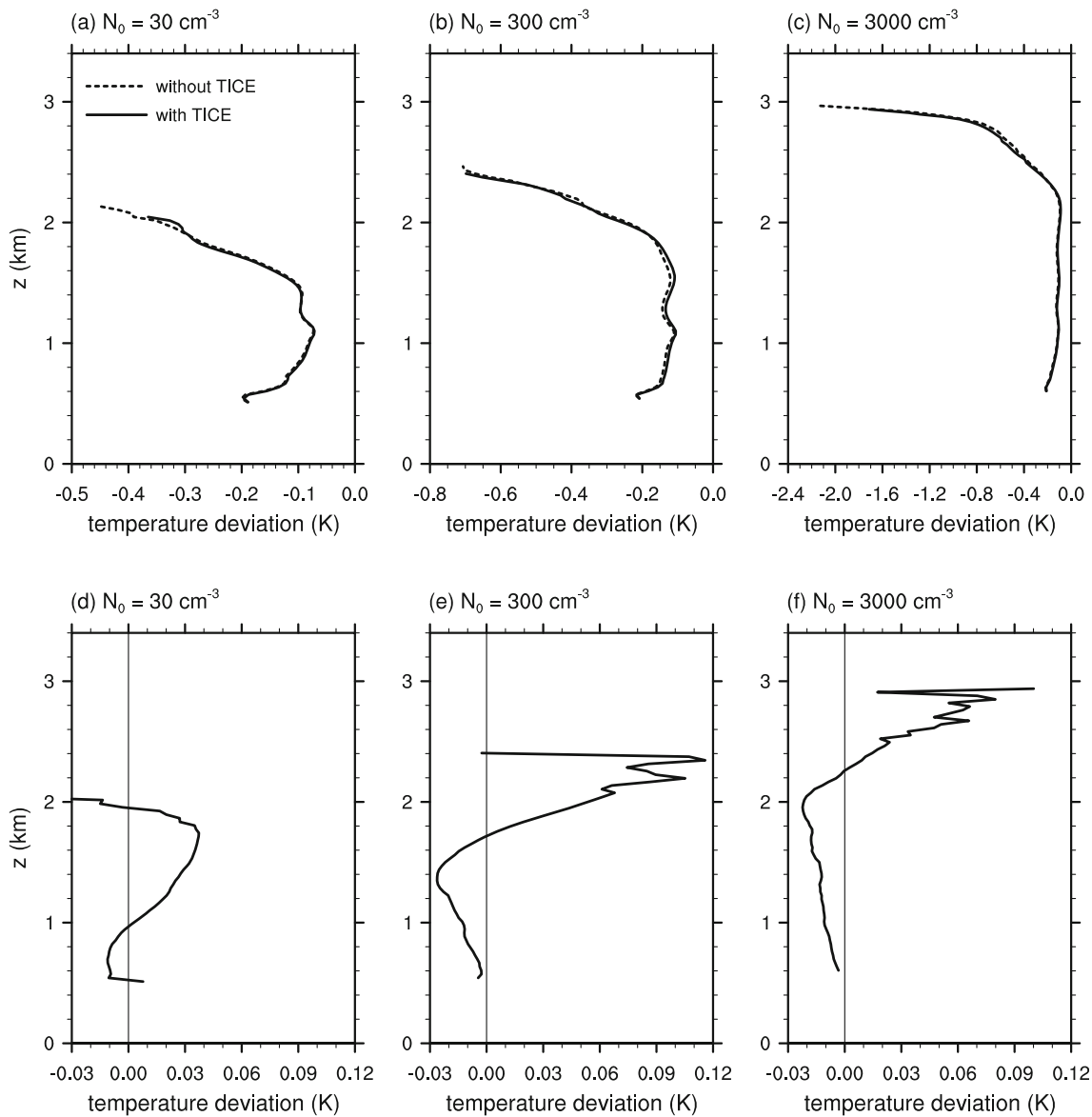


Fig. 11 Vertical profiles of temperature difference between cloudy grids and cloud-free grids. $N_0 =$ (a) 30 cm^{-3} , (b) 300 cm^{-3} , and (c) 3000 cm^{-3} . (d)–(f) are the same as (a)–(c) but for the in-cloud temperature difference between the cases with and without TICE

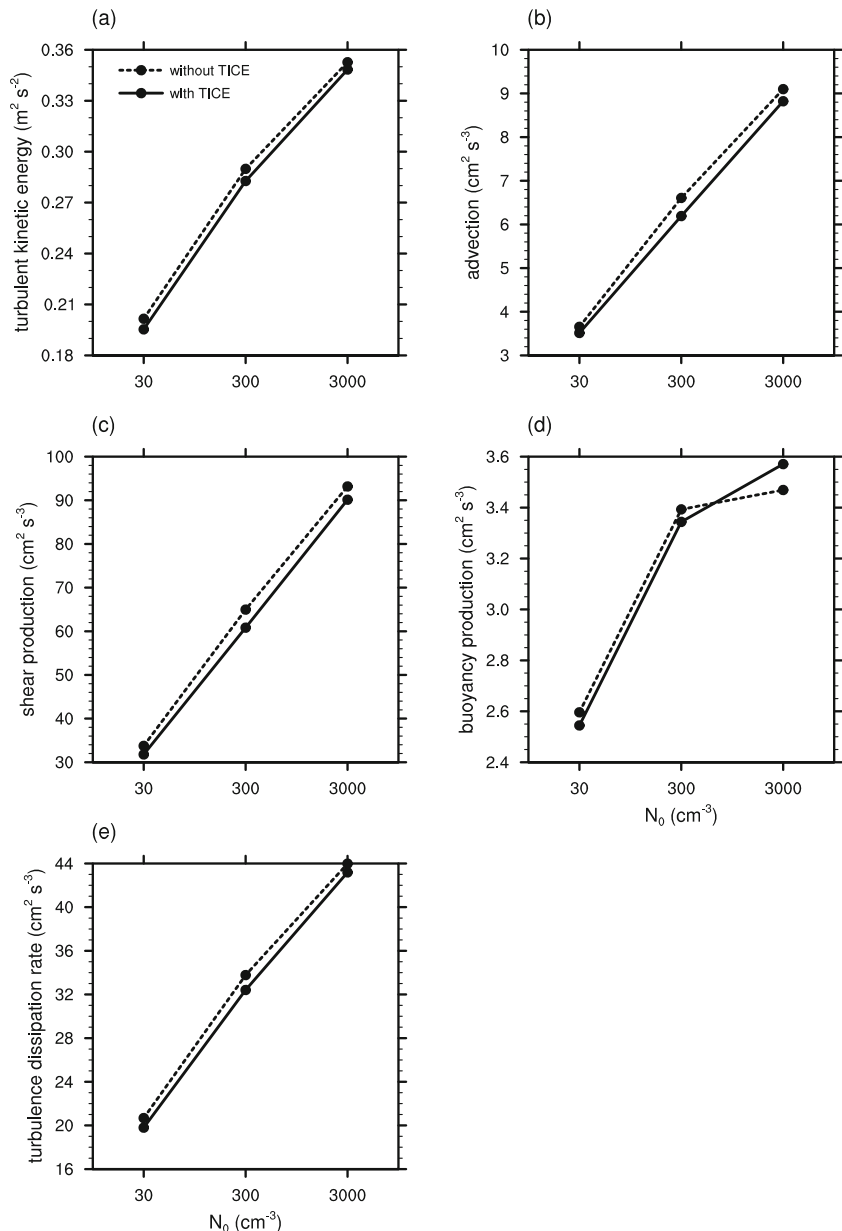
buoyancy production. The magnitude of shear production is approximately 10 times the magnitude of advection, and the magnitude of buoyancy production is much smaller than that of shear production. The shear production decreases due to TICE under all aerosol number concentrations, whereas the difference in buoyancy production due to TICE is small and varies depending on the aerosol number concentration. Therefore, it can be concluded that the decrease in TKE due to TICE is largely caused by the decrease in shear production. The decreased evaporative cooling due to TICE induces the more stabilized atmosphere and the decrease in vertical motion in the clouds (Figs. 10a and 11). In addition to the vertical velocity, the variance of vertical velocity averaged in the clouds is also decreased (Fig. 10b). These decreases in the

average and variance of vertical velocity are likely to induce the decrease in the shear production of TKE.

Aerosol-cloud-precipitation interactions comprise important problems in shallow convection (e.g., Xue et al. 2008; Feingold et al. 2010; Koren and Feingold 2011). Recent modeling studies have shown that precipitation organizes an open cellular structure and induces new convection around the precipitating area (e.g., Xue et al. 2008). Because TICE increases the surface precipitation (Fig. 3), it might be possible that the increased precipitation affects the precipitation-induced cloud development.

Figure 13 shows the snapshots of low-level vertical velocity, albedo, and surface precipitation rate at an arbitrary instance in the latter part of the model integration ($t = 9 \text{ h}$). It

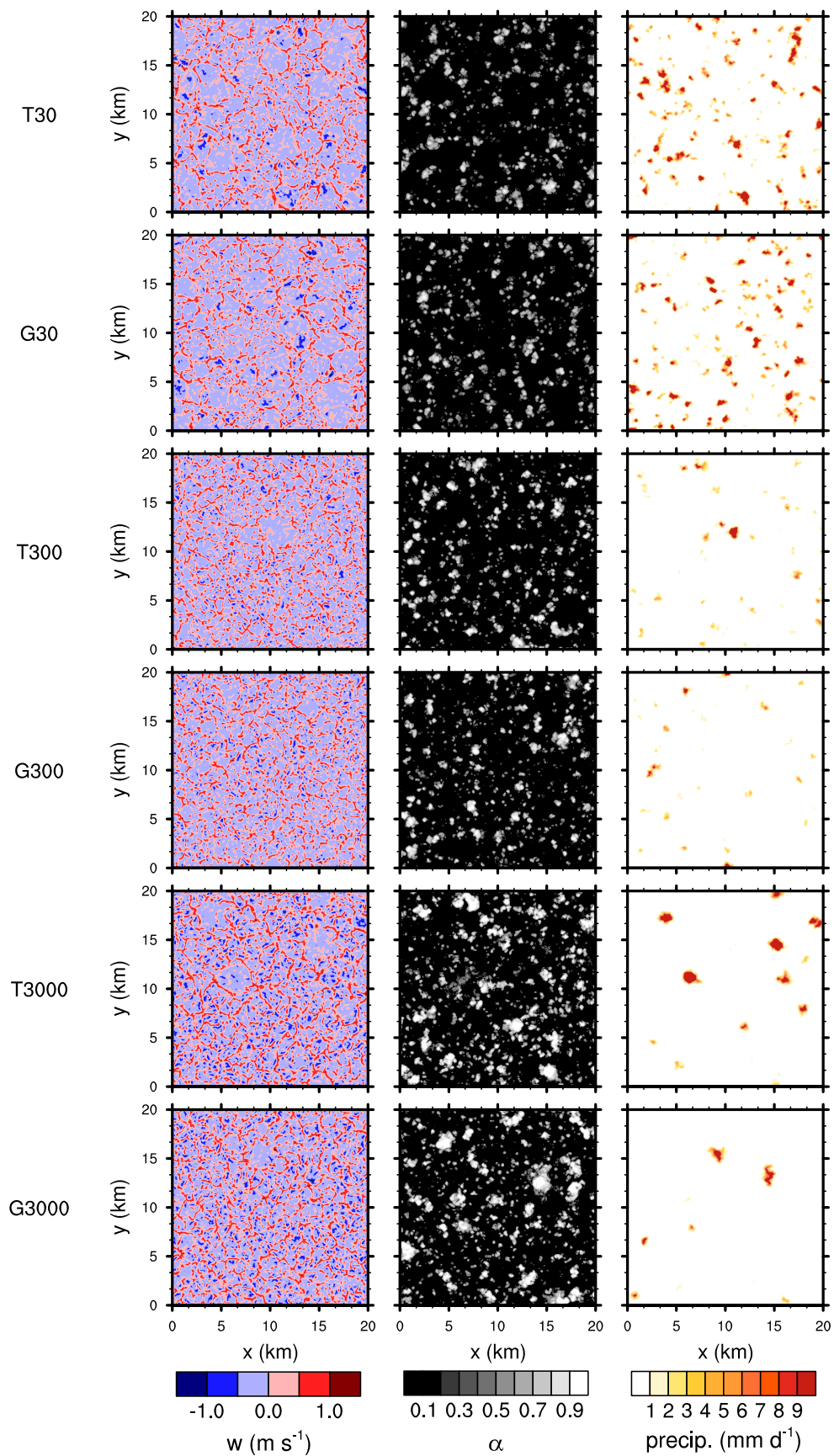
Fig. 12 (a) Turbulent kinetic energy (TKE), (b) advection of TKE, (c) shear production of TKE, (d) buoyancy production of TKE, and (e) turbulence dissipation rate averaged over the cloudy grids and for the last 3 h



is clearly seen that precipitation induces downdrafts and a wide cloud-free area which is centered at the downdraft area and surrounded by the ring-type updrafts. This is similar to the results of previous studies (e.g., Xue et al. 2008; Wang and Feingold 2009). However, unlike the results of previous studies (e.g., Xue et al. 2008; Franklin 2014), the destabilization induced by the evaporative cooling and the increase in TKE in the sub-cloud layer is very small in this study (Figs. 8 and 12). In addition, when the time evolution of the low-level vertical velocity and surface precipitation rate fields are examined, it is revealed that the TICE-induced increased precipitation hardly affects the cloud structure. The ring-type updrafts form around the cold pool induced by precipitation, but those updrafts do

not seem to develop enough to produce secondary convection and precipitation when $N_0 = 300$ or 3000 cm^{-3} .

One possible reason for these small changes is related to the precipitation intensity. The average precipitation rate in the aforementioned studies is of the order of a few millimeters per day, while that in this study has orders of 10^{-1} and 10^{-3} – 10^{-2} mm per day when $N_0 = 300$ and 3000 cm^{-3} , respectively. Therefore, the precipitation intensity under these aerosol number concentrations is weak compared to that of previous studies, and the continuous reactions (secondary convection and precipitation) might be rarely observed. The precipitation intensity when $N_0 = 30 \text{ cm}^{-3}$ has an order similar to that of previous studies, but the difference in precipitation rate



◀ **Fig. 13** Snapshots of (left column) vertical velocity at $z = 180$ m, (middle column) albedo, and (right column) surface precipitation rate at $t = 9$ h for each simulation case

induced by TICE is so small that the difference can produce little differences in cloud structure and morphology. As a result, TICE-induced increased precipitation affects minimally the development of the shallow cumulus in this study.

4 Summary and Conclusions

The effects of turbulence-induced collision enhancement (TICE) on precipitation and cloud radiative properties in precipitating shallow cumulus were numerically investigated through large-eddy simulations. Similar to some previous studies, the rainwater content is increased due to TICE, and moreover, TICE induces larger surface precipitation amount under all considered aerosol number concentrations. The relative increase in surface precipitation amount becomes more pronounced as the aerosol number concentration increases. The relative frequency of moderate to large surface precipitation amount is increased due to TICE when $N_0 = 300$ and 3000 cm^{-3} , whereas the relative frequency of largest surface precipitation amount is slightly decreased when $N_0 = 30 \text{ cm}^{-3}$. This decrease in the relative frequency of largest surface precipitation amount is likely to be related to the decrease in condensation amount in the strong updraft core areas due to a decrease in the first moment of drop size distribution. The drop size distributions at certain selected levels showed that TICE tends to decrease the number of small droplets and makes another critical point in the radius range of large drops, exhibiting a bimodal form of drop size distribution. On the other hand, a decrease in aerosol number concentration tends to shift the critical point in the radius range of small droplets to the radius of larger drops.

The increased mean drop radius and the decreased drop number concentration due to TICE result in a decrease in the first moment of drop size distribution, hence decreasing evaporation. This decrease in evaporation in turn increases the cloud fraction. At the same time, the cloud optical thickness, which is proportional to the second moment of drop size distribution, decreases due to TICE. These two changes offset each other so the domain-averaged albedo is little affected due to TICE. In addition, the decrease in evaporation particularly near the cloud top induces the less destabilized atmosphere in the clouds, hence causing a decrease in in-cloud vertical velocity and also a decrease in cloud top height. The decreased cloud top height and the increased cloud fraction offset each other so the change in domain-averaged outgoing longwave radiation due to TICE is not large.

On the feedback of TICE, in addition to the averaged vertical velocity, the variance of vertical velocity is also decreased

due to TICE mainly because of the reduced evaporative cooling. The decrease in the averaged and variance of vertical velocity induces a decrease in shear production of turbulent kinetic energy (TKE). While the shear production is predominant over the buoyancy production, the decrease in shear production results in a decrease in TKE. Therefore, TICE acts to produce a negative feedback.

Complex interactions among aerosols, clouds, and precipitation have been considered important in understanding the development of shallow cumulus. Particularly, aerosol-induced changes in precipitation are known to affect the evolution of secondary convection and precipitation. It seems that TICE-induced changes in precipitation have relatively small effects on the changes in cloud structure, mainly because relatively large changes in precipitation due to TICE are observed when the precipitation amount is very small and relatively small changes in precipitation due to TICE are observed when the precipitation amount is moderate.

Overall, the effects of TICE are clearly observed in precipitation, and the effects tend to be larger as the aerosol number concentration increases. However, the effects of TICE on cloud radiative properties are shown to be small. These small changes are partially due to offsets or negative feedback among numerous processes that affect the cloud radiative properties. However, these changes certainly depend on environmental conditions and further studies are needed. In addition, the turbulence-induced entrainment/detrainment around the cloud edges remains poorly understood. More follow-up studies are required to investigate the effects of turbulence more distinctly.

Acknowledgements The authors are grateful to two anonymous reviewers for providing valuable comment on this work. The first and second authors were funded by the Korea Meteorological Administration Research and Development Program under grant KMIPA 2015-5190. The authors thank supercomputer management division of the Korea Meteorological Administration for providing us with the supercomputer resource.

Appendix

The Moments of Drop Size Distribution

In this study, the k th moment of drop size distribution M_k is defined as

$$M_k = \sum_{i=1}^{\Lambda} r_i^k N_i,$$

where Λ is the largest bin number and r_i and N_i are the drop radius and drop number concentration in the i th bin, respectively. It is noted that the moments of drop size distribution are defined either for the drop mass or for the drop radius. In this

study, the moments of drop size distribution are defined for the drop radius due to usefulness. TICE enhances the collision between drops, thus resulting in an increase in drop size but a decrease in drop number concentration. Therefore, assuming that the liquid water content (the third moment of drop size distribution) is unchanged, the k th moment of drop size distribution for k smaller than 3 decreases but that for k larger than 3 increases due to TICE. For example, the zeroth moment (the drop number concentration), the first moment (the sum of drop radius), and the second moment (proportional to the sum of drop cross section) decrease, but the sixth moment (the radar reflectivity) increases due to TICE.

References

- Ayala, O., Rosa, B., Wang, L.-P.: Effects of turbulence on the geometric collision rate of sedimenting droplets. Part 2. Theory and parameterization. *New J. Phys.* **10**, 075016 (2008). <https://doi.org/10.1088/1367-2630/10/7/075016>
- Beard, K.V.: Terminal velocity and shape of cloud and precipitation drops aloft. *J. Atmos. Sci.* **33**, 851–864 (1976)
- Beard, K.V., Ochs, H.T.: Collisions between small precipitation drops. Part II: formulas for coalescence, temporary coalescence, and satellites. *J. Atmos. Sci.* **52**, 3977–3996 (1995)
- Benmoshe, N., Pinsky, M., Pokrovsky, A., Khain, A.: Turbulent effects on the microphysics and initiation of warm rain in deep convective clouds: 2-D simulations by a spectral mixed-phase microphysics cloud model. *J. Geophys. Res.* **117**, D06220 (2012). <https://doi.org/10.1029/2011JD016603>
- Berry, E.X., Reinhardt, R.L.: An analysis of cloud drop growth by collection: part II. Single initial distribution. *J. Atmos. Sci.* **31**, 1825–1831 (1974)
- Bleck, R.: A fast approximative method for integrating the stochastic coalescence equation. *J. Geophys. Res.* **75**, 5165–5171 (1970)
- Bott, A.: A flux method for the numerical solution of the stochastic collection equation: extension to two-dimensional particle distributions. *J. Atmos. Sci.* **57**, 284–294 (2000)
- Costa, S.M.S., Shine, K.P.: An estimate of the global impact of multiple scattering by clouds on outgoing long-wave radiation. *Q. J. R. Meteorol. Soc.* **132**, 885–895 (2006)
- Feingold, G., Koren, I., Wang, H., Xue, H., Brewer, W.A.: Precipitation-generated oscillations in open cellular cloud fields. *Nature* **466**, 849–852 (2010)
- Feingold, G., Koren, I., Yamaguchi, T., Kazil, J.: On the reversibility of transitions between closed and open cellular convection. *Atmos. Chem. Phys.* **15**, 7351–7367 (2015)
- Feingold, G., McComiskey, A., Yamaguchi, T., Johnson, J.H., Carslaw, K.S., Schmidt, K.S.: New approaches to quantifying aerosol influence on the cloud radiative effect. *Proc. Natl. Acad. Sci. U. S. A.* **113**, 5812–5819 (2016)
- Franklin, C.N.: A warm rain microphysics parameterization that includes the effect of turbulence. *J. Atmos. Sci.* **65**, 1795–1816 (2008)
- Franklin, C.N.: The effects of turbulent collision-coalescence on precipitation formation and precipitation-dynamical feedbacks in simulations of stratocumulus and shallow cumulus convection. *Atmos. Chem. Phys.* **14**, 6557–6570 (2014)
- Franklin, C.N., Vaillancourt, P.A., Yau, M.K., Bartello, P.: Collision rates of cloud droplets in turbulent flows. *J. Atmos. Sci.* **62**, 2451–2466 (2005)
- Grabowski, W.W., Wang, L.-P.: Growth of cloud droplets in a turbulent environment. *Annu. Rev. Fluid Mech.* **45**, 293–324 (2013)
- Grabowski, W.W., Wang, L.-P., Prabha, T.V.: Macroscopic impacts of cloud and precipitation processes on maritime shallow convection as simulated by a large eddy simulation model with bin microphysics. *Atmos. Chem. Phys.* **15**, 913–926 (2015)
- Houze Jr., R.A.: *Cloud dynamics*, 2nd edn. Academic Press, Oxford (2014)
- Jiang, Q., Wang, S.: Aerosol replenishment and cloud morphology: a VOCAL example. *J. Atmos. Sci.* **71**, 300–311 (2014)
- Khain, A.P., Ovtchinnikov, M., Pinsky, M., Pokrovsky, A., Krugliak, H.: Notes on the state-of-the-art numerical modeling of cloud microphysics. *Atmos. Res.* **55**, 159–224 (2000)
- Khain, A.P., BenMoshe, N., Pokrovsky, A.: Factors determining the impact of aerosols on surface precipitation from clouds: an attempt at classification. *J. Atmos. Sci.* **65**, 1721–1748 (2008)
- Khain, A., Rosenfeld, D., Pokrovsky, A., Blahak, U., Ryzhkov, A.: The role of CCN in precipitation and hail in a mid-latitude storm as seen in simulations using a spectral (bin) microphysics model in a 2D dynamic frame. *Atmos. Res.* **99**, 129–146 (2011)
- Köhler, H.: The nucleus in and the growth of hygroscopic droplets. *Trans. Faraday Soc.* **32**, 1152–1161 (1936)
- Koren, I., Feingold, G.: Aerosol-cloud-precipitation system as a predator-prey problem. *Proc. Natl. Acad. Sci. U. S. A.* **108**, 12227–12232 (2011)
- Kunnen, R.P.J., Siewert, C., Meinke, M., Schröder, W., Beheng, K.D.: Numerically determined geometric collision kernels in spatially evolving isotropic turbulence relevant for droplets in clouds. *Atmos. Res.* **127**, 8–21 (2013)
- Lee, H., Baik, J.-J.: Effects of turbulence-induced collision enhancement on heavy precipitation: the 21 September 2010 case over the Korean peninsula. *J. Geophys. Res. Atmos.* **121**, 12319–12342 (2016)
- Lee, H., Baik, J.-J.: A physically based autoconversion development. *J. Atmos. Sci.* **74**, 1599–1616 (2017)
- Lee, H., Baik, J.-J., Han, J.-Y.: Effects of turbulence on warm clouds and precipitation with various aerosol concentrations. *Atmos. Res.* **153**, 19–33 (2015)
- Low, T.B., List, R.: Collision, coalescence, and breakup of raindrops. Part II: parameterization of fragment size distributions. *J. Atmos. Sci.* **39**, 1607–1618 (1982)
- Mlawer, E.J., Taubman, S.J., Brown, P.D., Iacono, M.J., Clough, S.A.: Radiative transfer for inhomogeneous atmosphere: RRTM, a validated correlated-k model for the long-wave. *J. Geophys. Res.* **102**, 16663–16682 (1997)
- Ogura, Y., Takahashi, T.: The development of warm rain in a cumulus cloud. *J. Atmos. Sci.* **30**, 262–277 (1973)
- Pinsky, M., Khain, A., Shapiro, M.: Collision efficiency of drops in a wide range of Reynolds numbers: effects of pressure on spectrum evolution. *J. Atmos. Sci.* **58**, 742–764 (2001)
- Pinsky, M., Khain, A.P., Krugliak, H.: Collisions of cloud droplets in a turbulent flow. Part V: application of detailed tables of turbulent collision rate enhancement to simulation of droplet spectra evolution. *J. Atmos. Sci.* **65**, 357–374 (2008)
- Pruppacher, H.R., Klett, J.D.: *Microphysics of Clouds and Precipitation*, 2nd edn. Kluwer Academic Publishers, Dordrecht (1997)
- Riechelmann, T., Noh, Y., Raasch, S.: A new method for large-eddy simulations of clouds with Lagrangian droplets including the effects of turbulent collision. *New J. Phys.* **14**, 065008 (2012). <https://doi.org/10.1088/1367-2630/14/6/065008>
- Seifert, A., Khain, A., Blahak, U., Beheng, K.D.: Possible effects of collisional breakup on mixed-phase deep convection simulated by a spectral (bin) cloud model. *J. Atmos. Sci.* **62**, 1917–1931 (2005)
- Seifert, A., Nuijens, L., Stevens, B.: Turbulence effects on warm-rain autoconversion in precipitating shallow convection. *Q. J. R. Meteorol. Soc.* **136**, 1753–1762 (2010)
- Skamarock, W.C., Klemp, J.B., Dudhia, J., Gill, D.O., Barker, D.M., G. Duda, M., Huang, X.-Y., Wang, W., Powers, J.G.: A description of

- the Advanced Research WRF version 3. NCAR Technical Note, NCAR/TN-475+STR, NCAR (2008)
- Twomey, S.: The nuclei of natural cloud formation. Part II: The supersaturation in natural clouds and the variation of cloud droplet concentration. *Pure Appl. Geophys.* **43**, 243–249 (1959)
- vanZanten, M.C., Stevens, B., Nuijens, L., Siebesma, A.P., Ackerman, A.S., Burnet, F., Cheng, A., Couvreux, F., Jiang, H., Khairoutdinov, M., Kogan, Y., Lewellen, D.C., Mechem, D., Nakamura, K., Noda, A., Shipway, B.J., Slawinska, J., Wang, S., Wyszogrodzki, A.: Controls on precipitation and cloudiness in simulations of trade-wind cumulus as observed during RICO. *J. Adv. Model. Earth Syst.* **3**, M06001 (2011). <https://doi.org/10.1029/2011MS000056>
- Wang, H., Feingold, G.: Modeling mesoscale cellular structures and drizzle in marine stratocumulus. Part I: Impact of drizzle on the formation and evolution of open cells. *J. Atmos. Sci.* **66**, 3237–3256 (2009)
- Wang, L.-P., Grabowski, W.W.: The role of air turbulence in warm rain initiation. *Atmos. Sci. Lett.* **10**, 1–8 (2009)
- Wyszogrodzki, A.A., Grabowski, W.W., Wang, L.-P., Ayala, O.: Turbulent collision-coalescence in maritime shallow convection. *Atmos. Chem. Phys.* **13**, 8471–8487 (2013)
- Xue, H., Feingold, G., Stevens, B.: Aerosol effects on clouds, precipitation, and the organization of shallow cumulus convection. *J. Atmos. Sci.* **65**, 392–406 (2008)
- Zhang, Y., Stevens, B., Ghil, M.: On the diurnal cycle and susceptibility to aerosol concentration in a stratocumulus-topped mixed layer. *Q. J. R. Meteorol. Soc.* **131**, 1567–1583 (2005)